THE ASTRONOMICAL JOURNAL, 118:2430–2441, 1999 November

HUBBLE SPACE TELESCOPE MEASUREMENTS OF THE EXPANSION OF NGC 6543: PARALLAX DISTANCE AND NEBULAR EVOLUTION[1]

DARREN S. REED AND BRUCE BALICK
Department of Astronomy, Box 351580, University of Washington, Seattle, WA 98150-1580
ARSEN R. HAJIAN AND TRACY L. KLAYTON
US Naval Observatory, 3450 Massachusetts Avenue, NW, Washington, DC 20392-5420
STEFANO GIOVANARDI
Dipartimento di Astronomia, Università degli Studi di Bologna, I-40127 Bologna, Italy
STEFANO CASERTANO[2] AND NINO PANAGIA[2]
Space Telescope Science Institute, 3700 San Martin Drive, Baltimore, MD 21218
AND
YERVANT TERZIAN
Department of Astronomy and National Astronomy and Ionosphere Center, Cornell University, Ithaca, NY 14853
Received 1999 June 18; accepted 1999 July 21

ABSTRACT

The optical expansion parallax of NGC 6543 has been detected and measured using two epochs of *Hubble Space Telescope* images separated by a time baseline of only 3 years. We have utilized three separate methods of deriving the angular expansion of bright fiducials, with excellent agreement in the results. We combine our angular expansion estimates with spectroscopically obtained expansion velocities to derive a distance to NGC 6543 of 1001 ± 269 pc. The deduced kinematic age of the inner bright core of the nebula is 1039 ± 259 yr; however, the kinematic age of the polar caps that surround the core is larger—perhaps the result of deceleration or earlier mass ejection. The morphology and expansion patterns of NGC 6543 provide insight into a complex history of axisymmetric, interacting stellar mass ejections.

Key words: astrometry — planetary nebulae: individual (NGC 6543)

1. INTRODUCTION

Accurate distances to planetary nebulae (PNe) are critical for calculating the size, mass, luminosity, age, and other properties of PNe and their central stars. Distances to PNe are also crucial when studying properties of the Galaxy, such as the Galactic rotation, and scale height of their progenitor stars. In addition, distances are required to ascertain the planetary nebula luminosity function and use PNe as standard candles for cosmological distance studies (Ciardullo, Jacoby, & Ford 1988).

Despite being bright and containing (being dominated by) a rich line spectrum, PNe have distances that are remarkably ill-constrained. In fact, distances to many extragalactic PNe are better known than distances to most Galactic PNe. Many different distance measurement techniques have been applied to PNe in the past. Most have been statistical in nature, presuming that some property is common to the entire population (Hajian & Terzian 1996). The most commonly used PN distance estimation technique is known as the Shklovsky method (Shklovsky 1956) and assumes a constant ionized gas mass for all PNe. Unfortunately, these statistical techniques generate errors that are large, often a factor of 2 or more, as reviewed by Terzian (1997). For the Shklovsky method, $D \propto M_i^{0.4}$, where D is the nebular distance and M_i the ionized mass. Since PNe progenitor masses can span a factor of ≈ 10, assuming that M_i scales with the progenitor mass, distance errors of several hundred percent are typical.

The most reliable distance measurements for PNe so far have been achieved by measuring their expansion parallaxes (Terzian 1997). PN shell expansion velocities are typically ~ 10 km s^{-1}, or ~ 2 mas yr^{-1} at distances of ~ 1 kpc. Expansion parallax distance determinations require two epochs of image data separated by a time baseline $\gtrsim 1$ yr, which can be used to measure the angular expansion "parallax," $\dot{\theta}$, of a fiducial feature. The physical expansion velocity of the features must be spectroscopically obtained and converted to a tangential velocity, $v_\perp$ (i.e., the component of the velocity normal to the line of sight), using a spatiokinematic model of the nebula. Then the distance to a PN can be computed directly by dividing $v_\perp$ by $\dot{\theta}$ (Hajian, Terzian, & Bignell 1993).

Distances to nine PNe have been measured using radio images from the Very Large Array (VLA) at different epochs (Masson 1989a, 1989b; Gómez, Rodríguez, & Moran 1993; Hajian et al. 1993; Hajian, Terzian, & Bignell 1995; Hajian & Terzian 1996; Haryadi & Seaquist 1998). One attempt has been made to measure the expansion of NGC 6543 using the VLA. However, this expansion parallax measurement was unsuccessful because of insufficient image quality in the radio-wavelength data (Hajian & Terzian 1996).

The many well-defined, optically bright features of NGC 6543 serve as ideal fiducials in measuring its angular expansion. The ability to measure the expansions of individual features within this extraordinary nebula provides us with a way to sort through the nebula's recent history, to probe the mass ejection behavior of its nucleus, and to directly determine the distance to this PN.

[1] Based on observations made with the NASA/ESA *Hubble Space Telescope*, obtained from the data archive at the Space Telescope Science Institute, which is operated by the Association of Universities for Research in Astronomy, Inc., under NASA contract NAS 5-26555.

[2] On assignment from the Space Science Department of ESA.

As discussed by Hajian et al. (1995), the optical expansion of a PN is particularly detectable and is measurable with high accuracy (<25%) using the *Hubble Space Telescope* (*HST*). In this paper, we report the detection of the systematic expansion of NGC 6543 between 1994 and 1997 from *HST* archival observations. To quantify the magnitude of the angular expansion rate, we present three separate astrometric analyses of these recorded images. These observations, along with a spatiokinematic model of the nebula derived from independent measurements of the Doppler velocity, permit three direct distance determinations, all of which are in excellent agreement.

In addition, the expansion pattern reveals that the kinematic ages of features approximately scale with their angular size. This provides insight into the highly organized and orchestrated mass-loss history of the nucleus, presently a Wolf-Rayet Of star (Heap & Augensen 1987). This two-in-one paper discusses both the distance to and the nebular evolution of NGC 6543.

2. OBSERVATIONS

The bright core of NGC 6543 just fills the higher resolution Planetary Camera of the Wide Field Planetary Camera 2 (WFPC2), whose projected pixel size is 45.5 mas. Archived unsaturated *HST* narrowband images from general observer (GO) program 5403 and corresponding calibration images from GO program 6943 were used for this study (Table 1). The data epochs are separated by 35 months. Images through F502N (hereafter [O III]; F656N, Hα; and F673N, [S II]) filters were obtained at both epochs. The use of the same instrumentation for the two epochs, albeit at differing orientations, reduces systematic errors.

Measurements of the expansion were based solely on images in the [O III] 502 nm and [S II] 673 nm lines. The [O III] image is optimal for this study since it is characterized by well-defined, bright structures with excellent signal-to-noise ratios in the WFPC2 images. The Hα images appear essentially redundant to their [O III] counterparts. For this reason the Hα images were not analyzed. The [S II] images were used to confirm the expansion measurements from the [O III] images and to investigate the proper motions of specific, bright, low-ionization features.

The pointing and orientation of the *HST* were different for the 1994 and 1997 observations. Therefore, after cosmic rays were removed and the relative image intensities were calibrated, the images had to be regridded to a common center and orientation. We used the IRAF tasks DRIZZLE, IMSHIFT, and ROTATE to remove geometric distortions, align, and rotate the images. The shifts and rotations were dithered until patterns of residuals of the corresponding images from the two epochs showed no trace of alignment or orientation errors. We estimate the accuracy of the alignment to be $\lesssim 0.05$ pixels (2 mas) and the orientation to be $\sim 0\overset{\circ}{.}1$.

3. DATA REDUCTION AND RESULTS

3.1. *Methodology*

Blinking of the 1994 and 1997 images shows clearly that the nebula has changed its scale size (i.e., the pattern changes are radial). Our strategy was therefore to average shifts in the locations of fiducials on equal and opposite sides of the nucleus (along radial lines) using various methods.

The angular expansion rate, $\dot{\theta}$, is best measured using fiducials with narrow peaks and/or sharp edges. In our analysis, we concentrated on the edges of several nebular features shown in Figure 1. Using the nomenclature of Miranda & Solf (1992, hereafter MS92), we analyzed the "P.A. 25° ellipse" (E25) and the "P.A. 105° ellipse" (E105). In the outer regions, we were able to measure the motion of the bright polar caps and the faint polar condensations, referred to as DD′ and FF′, respectively, in MS92. These structures are identified in Figure 1.

We used three methods to extract $\dot{\theta}$ from the images. The most direct approach, called the profile method, is to compare one-dimensional radial brightness distributions, or profiles, from images of two epochs taken with the same filter. The relative positions of sharp nebular features are found by analyzing the flux gradients in the radial profiles in the residual image of the two epochs, as pioneered by Masson (1986). This method allows $\dot{\theta}$ to be estimated along many one-dimensional "cuts" through the nebula. The random errors appear to be dominated by photon statistics.

A summary of the profile method can be found in Hajian et al. (1993, 1995) and in Hajian & Terzian (1996), referred to therein as the "expansion parallax algorithm." The analysis for *HST* images is identical to the analysis for VLA data except that *HST* data are not obtained in the Fourier plane. The method requires high signal-to-noise ratios in the residuals after the images of two epochs are subtracted, and it assumes no change in surface brightness or nebular shape. Using this method, $\dot{\theta}$ can be computed for any bright feature intersecting a radial cut:

$$\dot{\theta}_{\rm prof} = \Delta F / \nabla F \ , \qquad (1)$$

where ∇F is the flux gradient of the nebular feature and $\triangle F$ is the peak value of the difference map near the nebular feature. We take the uncertainty in expansion measurement along an individual profile to be equal to (1) the difference

TABLE 1

WFPC2 OBSERVATIONS OF NGC 6543

Filter	Exposure (s)	R.A. (J2000.0)	Decl. (J2000.0)	*HST* P.A. (deg)	Date	Proposal	Principal Investigator
[O III] (F502N).....	2 × 200, 2 × 600	17 58 28.08	66 37 59.26	274.105	1994 Sep 18	5403	J. P. Harrington
	200	17 58 28.91	66 38 14.82	305.434	1997 Aug 17	6943	S. Casertano
[S II] (F673N)	2 × 400	17 58 28.08	66 37 59.26	274.105	1994 Sep 18	5403	J. P. Harrington
	400	17 58 28.91	66 38 14.82	305.434	1997 Aug 17	6943	S. Casertano
Hα (F656N).....	200	17 58 28.08	66 37 59.26	274.105	1994 Sep 18	5403	J. P. Harrington
	200	17 58 28.91	66 38 14.82	305.434	1997 Aug 17	6943	S. Casertano

NOTE.—Units of right ascension are hours, minutes, and seconds, and units of declination are degrees, arcminutes, and arcseconds.

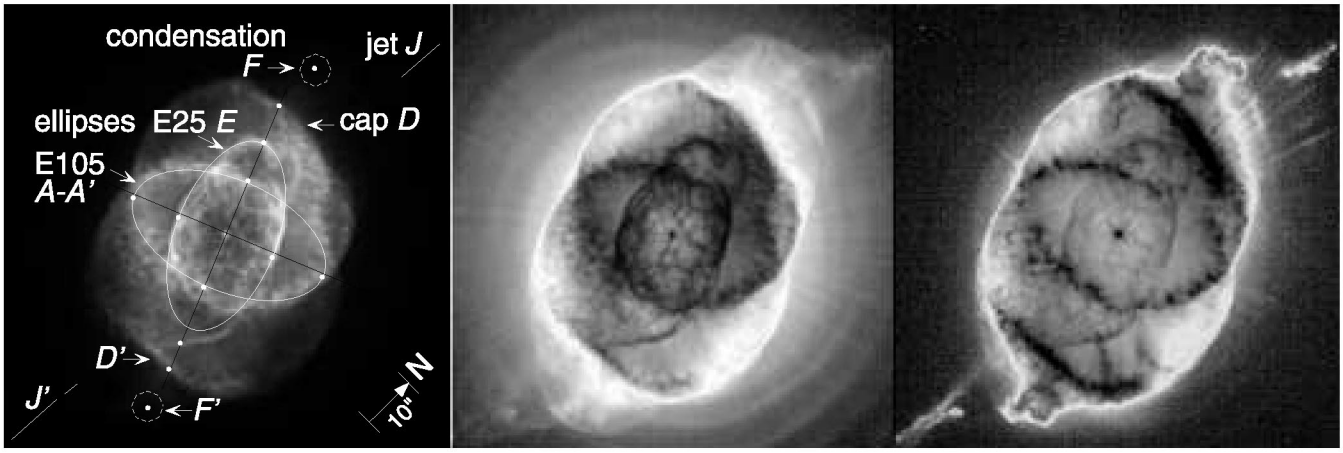

FIG. 1.—Images of NGC 6543. *Left*: Linear representation of the [O III] surface brightness. Various features are identified (MS92 terminology shown in italics). White dots show the locations of the radial fits of angular expansion rates of Table 2. *Middle*: A negative linear representation of the [O III] surface brightness superposed on a logarithmic display of the faint nebular background in the same *HST* image. *Right*: Like the center panel, but for the [N II] line. The [S II] image is noisier but otherwise similar to this panel.

between expansion rates inferred from the corresponding features on opposite sides of the nucleus or, where appropriate, (2) the unweighted mean and standard deviation of multiple cuts intersecting an extended structure.

The "radial fitting" method is a similar and somewhat redundant technique. The positions of bright nebular features along one-dimensional radial flux profiles are measured by performing Gaussian fits, by evaluating the flux-weighted centroid of a fiducial's peak, or by graphically measuring the shift of a sharp edge in each of the two epochs.

The radial fitting method has a somewhat increased potential for yielding expansion estimates for nebular features that are too faint for similar measurements with the profile method. This is because of the increased noise level in a difference map relative to the epoch maps ($\sqrt{2}$ for epoch maps with equal noise levels). The random errors of the measurement are dominated by the uncertainties in the fit, which include the judgment involved in defining a fiducial. For fits to peaks, the measurements of a Gaussian feature in a complicated environment are sensitive to choices of the edges and base of the fitted Gaussian curve. Great care is necessary to use the same procedures for the images of both epochs. Finding the relative positions of sharp edges is straightforward. It is done by overplotting the one-dimensional flux profiles of the two epochs and graphically measuring the radial displacement at multiple positions along the steep flux dropoffs of the edges. We assume a minimum 20% uncertainty in measured expansion rates since we employ the radial fitting method only once for each fiducial in each filter.

The magnification method is the simplest but least accurate of the methods. A magnification factor that minimizes the rms of the difference, or residual, image in the regions of the bright fiducial feature is applied to the first-epoch image.

For each emission line, [O III] and [S II], we used the IRAF task GEOTRAN to magnify the 1994 image by different magnification factors, M, in the range $1.001\times$ to $1.005\times$. For radial motions with no brightness changes, a given feature will disappear in the residual image after the magnified 1994 image is subtracted from the aligned 1997 image. We can then compute $\dot{\theta}$ using the following equation:

$$\dot{\theta}_{\rm mag,\ mas\ yr^{-1}} = \frac{(M-1)\theta_{\rm mas}}{2.92\ {\rm yr}}, \tag{2}$$

where θ is the angular distance from the nucleus to the feature.

The advantages of the magnification method are that the entire image is utilized, that the intuitive pattern recognition capability and judgment of the brain can be exploited, and that the residuals may uncover deviations from simple radial expansion in the complex nebula that would not easily be recognized in one-dimensional analyses of the brightness distribution. The major disadvantage to the magnification method is that errors are difficult to quantify. We assume an uncertainty of 25% in our magnification method expansion rates.

3.2. *Distance Estimates and Kinematic Ages*

Once $\dot{\theta}$ has been measured using the above methods, $v_\perp$ has been determined based on spectroscopic observations, and a spatiokinematic model has been used to convert radial into tangential velocities, the distance to the nebula in parsecs can be calculated:

$$D_{\rm pc} = 211 v_{\perp,\ {\rm km\ s^{-1}}}/\dot{\theta}_{\rm mas\ yr^{-1}}\ . \tag{3}$$

The tangential component of the expansion velocities of various features were taken from the detailed observations and the nebular models of MS92. In addition, the kinematic age, T, in years of a fiducial is given by

$$T = \theta_{\rm mas}/\dot{\theta}_{\rm mas\ yr^{-1}}\ . \tag{4}$$

We also note that a more accurate distance can be computed by taking all of the measured values of $\dot{\theta}$ into account (i.e., $\dot{\theta}$ at multiple position angles for multiple features, rather than just the minor axis of E25, which our distance is based upon). However, since (1) the only available kinematic information for NGC 6543 was obtained in an emission line, [N II] λ6584, that is different from the line(s) used to determine the astrometric expansion of the nebula,

[O III] λ5007 and [S II] $\lambda\lambda$(6717 + 6731), and the (2) uncertainty in the adopted expansion velocity is approximately $\sim$10%, we did not feel it was necessary to fit a complex spatiokinematic model to the data. This is more appropriate for positionally resolved velocities obtained in the summer of 1999.

We next discuss the measurements of $\dot{\theta}$ using all three methods. The results are compiled in Table 2. Also shown in the table is the expected value of $\dot{\theta}$, assuming a uniform nebular expansion whose rate is calibrated to the average measurement of $\dot{\theta}$ along the minor axis of E25 (see below).

For the [O III] images, we applied the profile analysis to various radial cuts through the nucleus in 10° increments, as shown in Figure 2. The resulting angular expansion rates are displayed in units of mas yr^{-1} wherever the profile intersects a bright, thin feature. For the [S II] images, we measured $\dot{\theta}$ along radial cuts through the central star at intervals of 2°, as shown in Figure 3. The residuals of the magnification method are shown in Figures 4 and 5, and the corresponding values of $\dot{\theta}$ are listed in Table 2.

The changes in the nebular structure are seen most clearly in the residual images of the unmagnified 1994–1997 image pairs (see Figs. 4 and 5, *top left*). Although the residuals are only about 1% of the image brightnesses, the patterns of change are quite clear. None of the residuals from any of these techniques yield evidence of nonradial motions.

The best estimates of the distance rely on sharply defined symmetric structures such as spheres or prolate ellipsoids with sharp edges. We capitalize on a geometric trick: the measurement of $\dot{\theta}$ along the minor axis of a prolate ellipsoid is ideal for deriving an expansion distance since no geometric correction for inclination is required. E25 is the optimum structure for expansion studies because of the prominent and sharp edges along its minor axis and its well-measured expansion velocity. E105 is somewhat more diffuse than E25, and the Doppler velocity mapping of MS92 has shown it to be a tilted circular ring rather than an prolate ellipsoid; however, it serves as a useful consistency check.

E25.—For the profile method, the best measured expansion rate of E25's minor axis in the [O III] images is $\dot{\theta}_{\rm prof} = 3.63 \pm 0.82$ mas yr^{-1}. Adopting the expansion velocity of MS92, 16.4 km s^{-1}, from the kinematic model described earlier in this section and a 10% velocity uncertainty results in a distance $D_{\rm E25} = 953 \pm 235$ pc. Based on a size of $\theta = 3\farcs6$ for the semiminor axis of E25, the kinematic age is $T_{\rm E25} = 990 \pm 223$ yr.

The radial fitting method was used on both the [O III] and the [S II] images. Using the IRAF command SPLOT, Gaussians were fitted to measure the shift of the fiducial features between the two epochs. For [S II], the radial cuts were offset slightly to avoid a bright cosmic ray $\sim 1\farcs5$ to the south of the central star.

We measured an angular expansion rate $\dot{\theta}_{\rm rad} = 3.36 \pm 0.86$ mas yr^{-1} for the minor axis of E25 using this method. The result agrees to within 10% with the result of the profile method. The kinematic model described above implies a distance $D_{\rm E25} = 1030 \pm 283$ pc. The corresponding kinematic age $T_{\rm E25} = 1070 \pm 274$ yr.

The magnification method yields very consistent results. The expansion of most of the inner core (within the intersection of E25 and E105) is well characterized by a single magnification factor midway between 1.0025 and 1.003. We adopt a value of 1.00275 and an error of 25% (i.e., $\dot{\theta}_{\rm mag} = 3.4 \pm 0.9$ mas yr^{-1}). Judging from the darkened residuals along E25, there may have been a slight decrease in surface brightness as well. The distance derived from the magnification method results is $D_{\rm E25} = 1021 \pm 288$ pc. We derive a kinematic age $T_{\rm E25} = 1057 \pm 280$ yr.

Combining the results for the minor axis of E25 with equal weights and averaging the errors, we derive a best-estimate distance $\bar{D} = 1001 \pm 269$ pc and a kinematic age

TABLE 2

ANGULAR EXPANSION RATES OF NGC 6543

FEATURE	ANGULAR DIAMETER (arcsec)	METHOD	$\dot{\theta}$ (mas yr^{-1}) [O III]	$\dot{\theta}$ (mas yr^{-1}) [S II]
E25 minor	7.2 (in [O III])	Profile	3.63 ± 0.82	
		Radial fit	3.36 ± 0.86	
		Magnitude	3.4 ± 0.9	
E25 major.....	16.1 (in [O III])	Profile	4.51 ± 0.85	
		Radial fit	1.95 ± 1.01	
		Magnitude	4.8 ± 1.2	
		Linear (Hubble) expectation	7.7	
E105 minor	9.0 (in [S II])	Profile	5.8 ± 1.5	
		Radial fit	3.98 ± 1.17	3.28 ± 0.7
		Magnitude	4.6 ± 1.2	4.6 ± 1.2
		Linear (Hubble) expectation	4.3	
E105 major	14.6 (in [S II])	Profile	7.2 ± 1.5	
		Radial fit	4.68 ± 2.34	8.59 ± 1.7
		Magnitude	7.5 ± 1.9	7.5 ± 1.9
		Linear (Hubble) expectation	7.0	
Polar caps DD′	21.2 (in [S II])	Profile	6.70 ± 1.37	6.94 ± 1.42
		Radial fit	6.56 ± 1.3	5.86 ± 1.2
		Magnitude	6.4 ± 1.6	6.4 ± 1.6
		Linear (Hubble) expectation	10.2	
Condensations FF′.....	24.7 (in [S II])	Radial fit		2.73 ± 1.64
		Magnitude		4.2 ± 1.1
		Linear (Hubble) expectation	11.9	

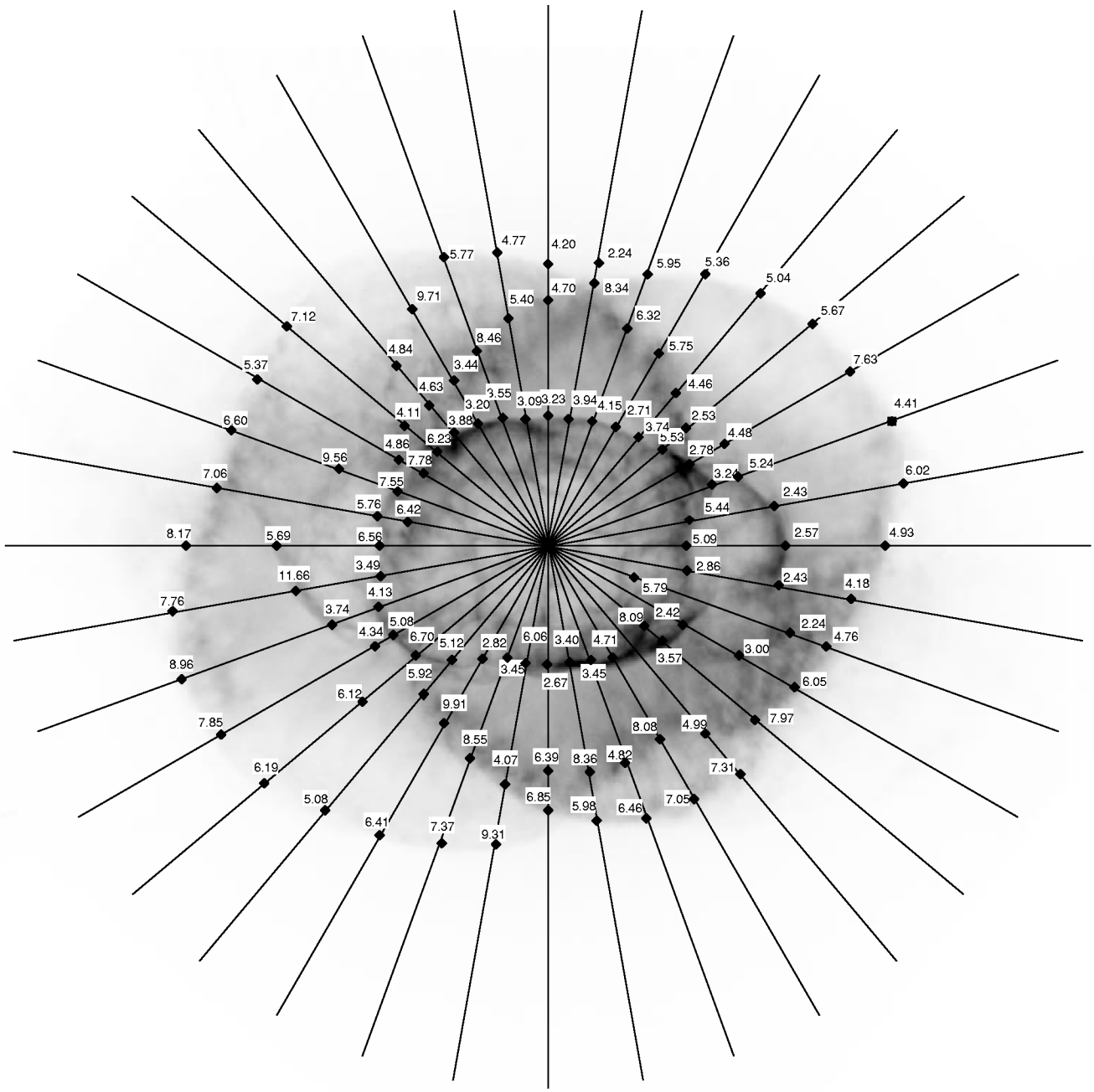

FIG. 2.—Linear representation of the [O III] surface brightness of NGC 6543 showing the location of the profiles analyzed in § 3.2. Values of the angular expansion rate in mas yr^{-1} are shown corresponding to the locations (*diamonds*) where the profile cuts intersect bright regions of the nebula.

$T = 1039 \pm 259$ yr. This conservative approach of averaging our uncertainties together is warranted because our measurements all rely on the same images and radial velocities and are, therefore, not statistically independent.

Next we consider the measurement of $\dot{\theta}$ along the major axis of E25. The structure at the ends of the major axis is much more poorly defined than that along the minor axis. Accordingly, the various techniques produce somewhat scattered results. We measure 4.51, 1.95, and ~ 5 mas yr^{-1} using the profile, radial, and magnification methods, respectively. The disagreement in the results is substantial. However, the important point is that on average all of the methods fall about a factor of 2 short of the expected result for uniform (Hubble law–like) expansion, 7.7 mas yr^{-1}. In other words, the kinematic age of the major axis of E25 is ~ 2000 yr.

Similarly, large expansion ages are obtained not just along the major axis of E25 but throughout the periphery of the core of NGC 6543 by almost all methods. Whether the peripheral structures are truly older than the material along the minor axis of E25 or whether the outer material is coeval and decelerated is an issue that will be addressed in § 4.

In principle, the major axis of E25 can be exploited to check the expansion distance since we are able to measure its expansion rate $\dot{\theta}$. After some consideration, we decided this would be a mistake for several reasons: (1) $\dot{\theta}$ must be corrected for inclination and the angle is uncertain; (2) the

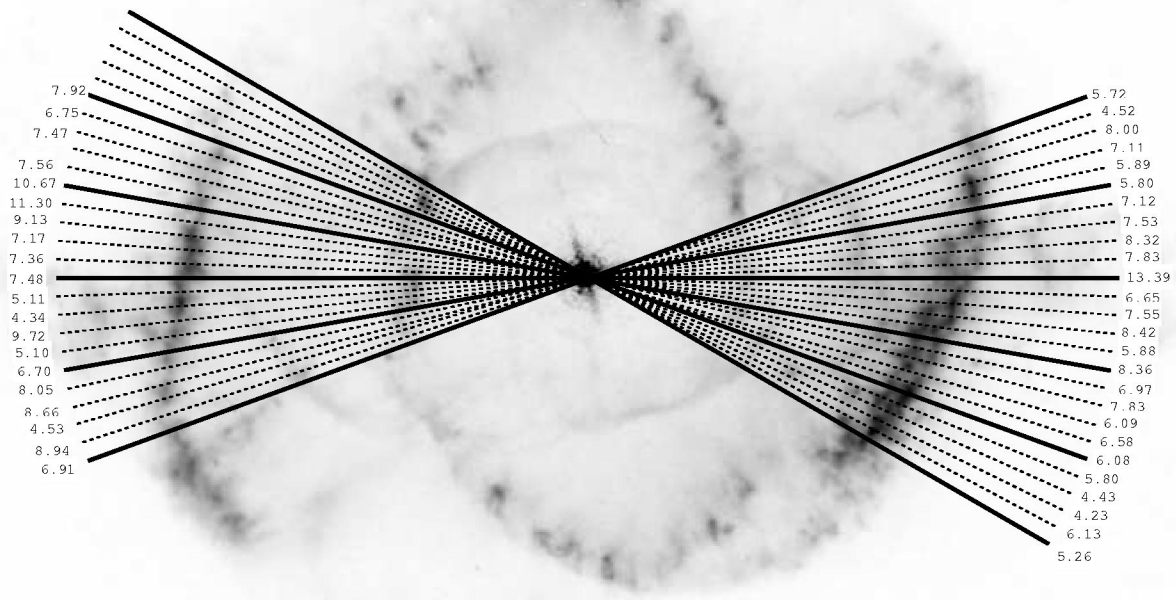

FIG. 3.—Same as Fig. 2, but for the [S II] surface brightness. Values shown correspond to the measured angular expansion rates in mas yr^{-1} where the profiles intersect the bright polar caps.

structure of E25 along its major axis is irregular and faint; (3) our data show that the ellipse E25 does not expand uniformly, as MS92 assumed, and that the major axis deviates the most from the uniform expansion pattern; and (4) there is some doubt that the tips of E25 are actually part of the same physical structure as the minor axis (Balick, Wilson, & Harrington 1999).

E105.—E105 has almost the same projected size and shape as E25, so it is tempting to use it to derive an independent distance to NGC 6543. However, E105 is lumpier and more diffuse, and measuring its size and expansion rate is commensurably more uncertain. In addition, its expansion velocity is not as well known.

All three methods again yield consistent results on the expansion rate of E105 along its major and minor axes. Moreover, those results concur with the expansion rates derived for E25. That is, the values of $\dot{\theta}$ for E105 follow a uniform Hubble law expansion relation based on the angular size and $\dot{\theta}$ that we measured for the minor axis of E25. This is comforting. This means that E105 and the minor axis of E25 share the same kinematic ages.

Let us now employ the MS92 model wherein E105 is a planar circular ring that surrounds E25 and shares the same symmetry axis. Since E105 is a tilted circular ring, the ring's expansion rate measured along its major axis, 7.1 ± 1.8 mas yr^{-1}, needs no geometric correction for tilt (this value is an average of the results of the various methods in Table 2). The measured expansion velocity is 28 km s^{-1} (MS92), and the derived distance D_{E105} is 832 ± 211 pc, where the errors in the expansion velocity (which may be substantial for this

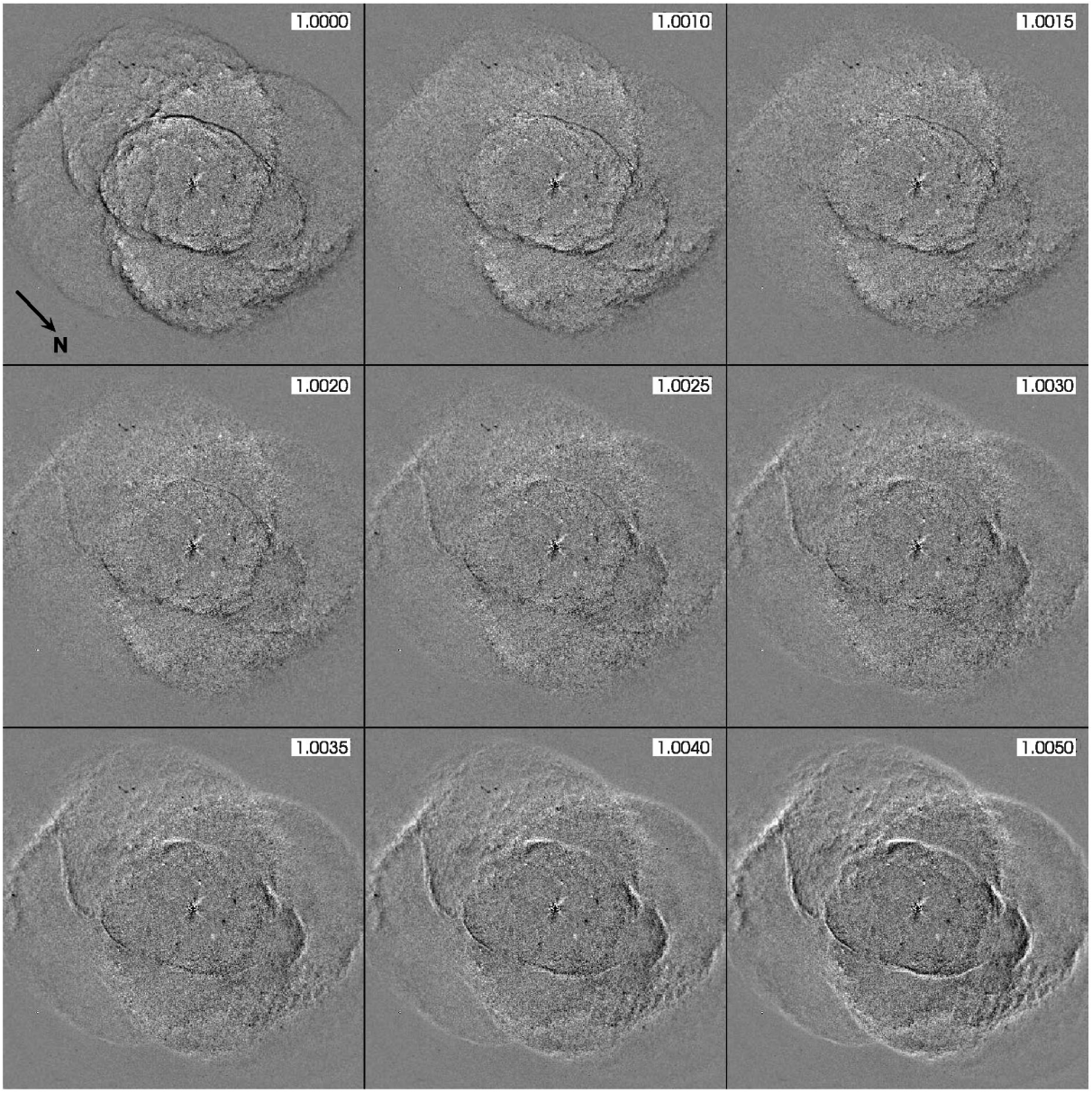

FIG. 4.—A montage of F502N ([O III]) residual images after the 1997 images were subtracted from magnified and aligned 1994 images. The magnification factors applied to the 1994 images are shown in the upper right corners of each panel.

feature) have been ignored. Satisfyingly, D_{E105} is consistent with $\bar{D}$.

Caps DD′.—The caps are lumpy complexes that lie within thin regions in the outermost extremities of the nebular core. The locations of the caps at the extreme edges of the core suggest that the pair of them lie in or near the plane of the sky. This means that their Doppler shifts should be, in principle, unmeasurable, and no distance can be estimated from them. On the other hand, this same geometry guarantees a straightforward computation of the kinematic age once the angular expansion rate of the caps has been measured.

If NGC 6543 expands uniformly at the rate determined from the minor axis of E25, then we would expect the caps to exhibit angular expansion rates $\gtrsim 10$ mas yr^{-1}. Using the profile method, we detected the signature of angular expansion from the polar caps in both [O III] and [S II]. In the case of [O III], the expansion rate of the polar caps averages to 6.70 ± 1.37 mas yr^{-1}. In the case of [S II], the average expansion of the polar caps is 6.94 ± 1.42 mas yr^{-1}. The discrepancy from uniform expansion lies well outside measurement errors.

These results are verified by the radial method, which yields expansion rates of 6.56 ± 1.3 and 5.86 ± 1.2 mas yr^{-1} for [O III] and [S II], respectively. The residuals of the caps are minimized for values of $1.0015 \lesssim M \lesssim 1.0020$ in both the [S II] and the [O III] images. Our value $M = 1.00175$ corresponds to a $\dot{\theta}$ of 6.4 ± 1.6 mas yr^{-1}, which agrees very well with the results from the other two methods.

When all three methods are averaged together, the caps have an expansion rate of 6.46 ± 1.4 mas yr^{-1}, which is more than a third smaller than the expected uniform expansion rate. They are characterized by a kinematic age of

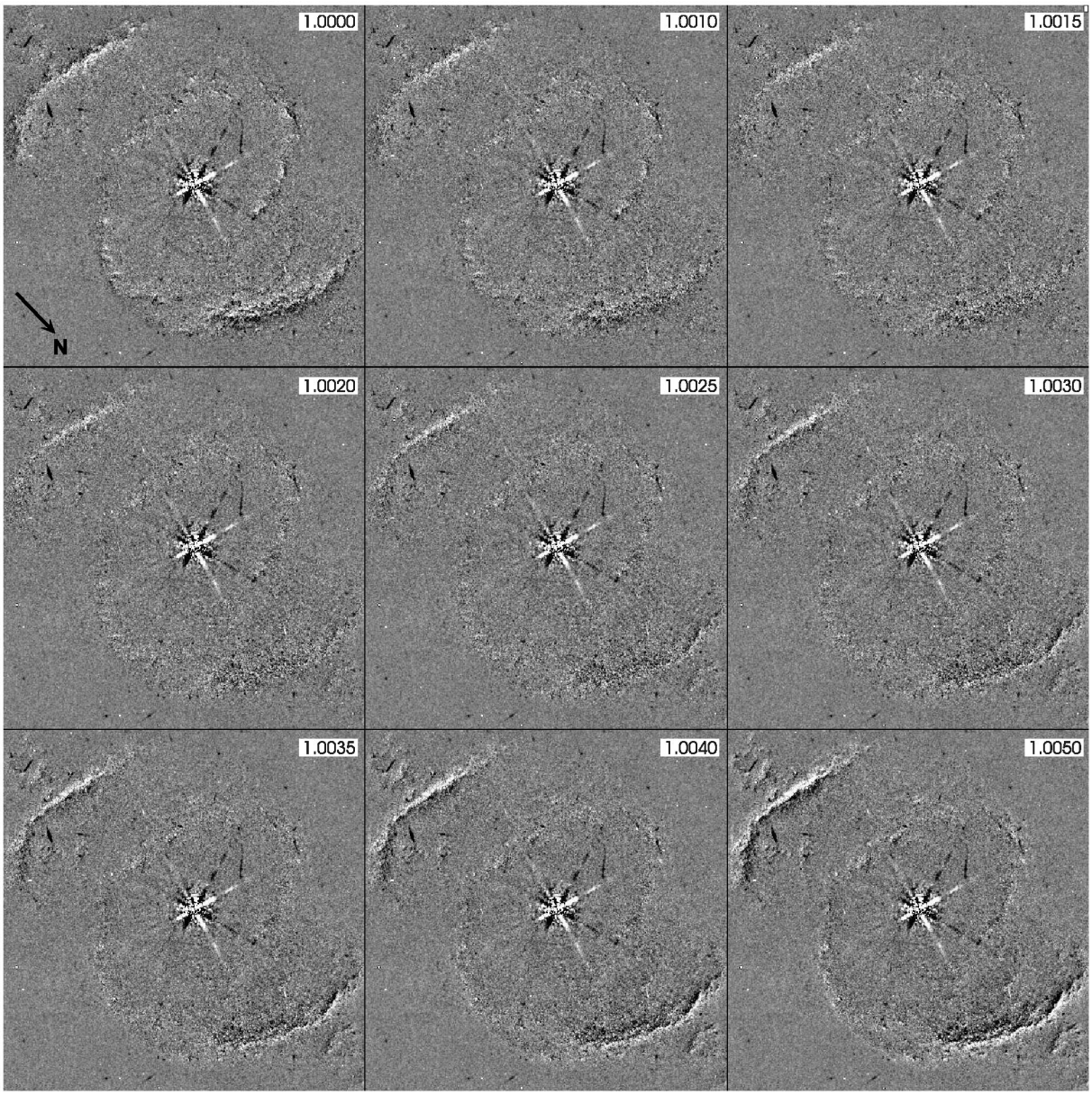

FIG. 5.—Same as Fig. 4, but for the F673N ([S II]) images

1628 ± 375 yr. The caps, like the major axis of E25, have significantly larger kinematic ages than the inner regions of E25.

Condensations FF′ and jets JJ′.—If the condensations follow the expansion rate of the minor axis of E25, then we expect to measure a large angular expansion rate, ~12 mas yr^{-1}. Yet their proper motions are barely discernible (Table 2 and Fig. 5). This is even more peculiar in light of their relatively large Doppler shifts, about ±25 km s^{-1} (MS92), which, after (presumably) large correction for inclination, suggest true space velocities ~42 km s^{-1} relative to the nucleus. It is therefore quite curious that their proper motions are so small.

Unfortunately, the roll angle of *HST* excluded the interesting polar jets JJ′ from the 1997 images. Future *HST* observations of NGC 6543 using the 1994 roll angle should allow measurement of their proper motion.

Decreasing expansion rates.—All of the methods seem to agree that the apparent expansion rates do not increase linearly with increasing radius, i.e., the core of NGC 6543 does not expand uniformly. Either the outer nebular gas is decelerating or it was ejected considerably earlier than was the gas within ~6″ of the nucleus. We shall return to these points below.

3.3. *Discussion of Distances and Methodologies*

Based primarily on E25, we have derived a distance to NGC 6543 of 1001 ± 269 pc. This result is consistent with the previous distance determinations of 1100, 1170, and 980 pc by Cudworth (1974), Castor, Lutz, & Seaton (1981), and Cahn, Kahler, & Stanghellini (1992), respectively, but it difers from the 640 pc distance computed by Daub (1982) by about 1.4 σ.

The various methods that we used to measure angular expansion rates all appear to be feasible. (The glaring exception is $\dot{\theta}_{\rm rad}$, measured for the E25 major axis in the [O III] line.) Indeed, based on the experience that we gained, it seems that proper motions of 0.25 pixels, or about 12 mas,

with the Planetary Camera can be measured with errors of order 20% when the signal is strong. This applies not only to images obtained under ideal conditions (same guide stars, centering, and spacecraft orientation) but under situations in which substantial regridding of the data and corrections for geometric distortions and cosmic rays are required.

According to the papers by Hajian et al. (1993, 1995) and Hajian & Terzian (1996), the profile method might even achieve accuracies of 2 mas under better conditions (sharper features, better control of the observations, ideal exposure durations, etc.) than those in this study. However, the ultimate technique would exploit the two dimensions of the image data, perhaps based on the optimum reduction of the residuals along various filamentary features or the nebula as a whole. Of course, at some point, expansion parallax studies will be limited by systematic errors in the WFPC2 detectors, but apparently this limit has not been reached for motions as small a few milliarcseconds.

However, the most severe limitation of any PN expansion distance method remains a combination of assumptions about the three-dimensional geometry of the target and the measurement of expansion velocities, especially with spatial resolutions obtainable from the ground in complex targets such as NGC 6543.

4. PROBING THE EVOLUTION OF NGC 6543

MS92 built a heuristic (empirical) model for the evolution of NGC 6543 from the best (ground-based) images available in 1991 and their detailed long-slit spectroscopy. They assumed that each feature in the core of the nebula was axisymmetric and uniformly expanding. Using the data and this assumption, they could derive the dimensions and inclination of each feature.

E25 was modeled as a closed, prolate ellipsoid, and E105 is a circular ring surrounding E25 in its equatorial plane. In their model, a second or "outer" thick ellipsoid surrounds the nebular core. Its inner edges are approximately delineated by the caps DD′ on its major axis and the projected tips of E105 along its minor axis. MS92 found that both E25 and the outer ellipsoid expand uniformly along nearly the same symmetry axis and inclination.

The newer and more detailed *HST* images require an entirely new geometric interpretation. Our heuristic model for the geometry of NGC 6543 is shown in Figure 6. We retain the idea of E25 as a prolate ellipsoid, albeit with numerous small bulges and irregularities near its tips. We are confident that E25 is a prolate ellipsoid for two reasons: (1) spectroscopic data of MS92 showed with high certainty that it is a closed ellipsoid and (2) the *HST* images are highly suggestive of a prolate ellipsoidal structure. The outer thick ellipsoid is replaced with a figure-eight outline of two roughly spherical bubbles with truncated outer regions where the caps are seen. E105 is situated at the locus where the bubbles are conjoined at the waist, much like a figure eight with a fat waist, or "fat eight." E25 forms one coherent structure, and E105 and the fat eight together form an ensemble that we denote the "conjoined bubbles."

Both E25 and the conjoined bubbles have sharp edges, which are nearly unresolved. If they are $\bar{T} \approx 1000$ yr old or older and if these sharp edges (which are strong nebular pressure gradients) were free to relax (expand) at their internal sound speed of 10 km s^{-1}, then they would be $\gtrsim 3 \times 10^{16}$ cm, or $\gtrsim 2''$, in diameter.

However, almost all of the features in the core of NGC 6543 have edges that are $\lesssim 0''.2$ thick, suggesting that they are constrained by some pressure, perhaps thermal or ram pressure. What is more, if the edges of the expanding features have been accreting material with low specific momentum, then they will have been decelerated. The farther they have traveled, the more they will have slowed, nicely in accord with the expansion patterns discussed in § 3.2. In any event, the growth patterns of the core of NGC 6543 provide a very interesting and useful glimpse into the physics of its formation and evolution, as we discuss next.

E25.—The standard concept of E25 as a wind-heated, thermally expanding bubble moving forward supersonically (about Mach 1.5) is compatible, on the whole, with its morphology, measured Doppler shifts, and pattern of angular expansion. The gas that the bubble has displaced and swept up is now compressed into the bright rim that outlines it. The leading shell seems to have developed thin-shell instabilities, or lumps, of small amplitude during its evolution. This happens because the outward flow of the thermally driven expanding bubble surface encounters dense regions upstream and bends around them, forming surface lumps. (However, the scale of the lumps is too small to allow studies of their individual expansion patterns.)

The 1994 and 1997 observations show that although E25 is likely a prolate ellipsoid, it is not expanding uniformly. Indeed, its expansion rate is smallest at its outermost tips. The expansion of the conjoined bubbles is more difficult to ascertain; however, its angular expansion rate is roughly that of E25. Therefore, the conjoined bubbles are older, more decelerated than E25, or both.

Lumpy ellipsoids like E25 are common in elliptical PNe such as NGC 6543. Close counterparts are seen in *HST* images of NGC 5882, 6826, and 6884, and, especially, NGC 7009 (Balick et al. 1998). In the last case, the bubble has essentially the same morphology as does E25. Emanating from the tips of the bubble in NGC 7009 are highly collimated gas jets with bright ansae at their termini. The symmetry axis of NGC 7009 appears to be oriented close to the plane of the sky. However, if viewed at an inclination of $\sim 30°$, the bubble, jets, and ansae would resemble E25 and the jets JJ′ in NGC 6543.

The elongated shape of E25 and the bubble of NGC 7009 are generally believed to be the consequence of a high-pressure waist of confining material that forces the thermally expanding bubble to grow most rapidly along the direction orthogonal to the disk (e.g., Icke, Balick, & Frank 1992). Thick disks or tori produce prolate ellipsoids because the expansion in a large equatorial region is hindered. Thin disks, on the other hand, produce pairs of figure-eight lobes as in the Homunculus of η Carinae (Morse et al. 1998) and the conjoined bubbles of NGC 6543, because the restricting material is confined to a narrow, dense region, while allowing free expansion in the rest of the nebula.

The concept of E25 as a thermally expanding bubble fails two tests. First, the torus that putatively constrains the equatorial growth of E25 should be situated astride the minor axis of E25 and probably interior to E105. Such a torus is readily discerned in NGC 7009. However, no such torus is apparent in NGC 6543, perhaps because of the confusion of brighter features nearby.

Second, the prolateness develops because the wind-driven bubbles expand fastest in the polar directions, where the upstream confining pressures are smallest. Therefore, the

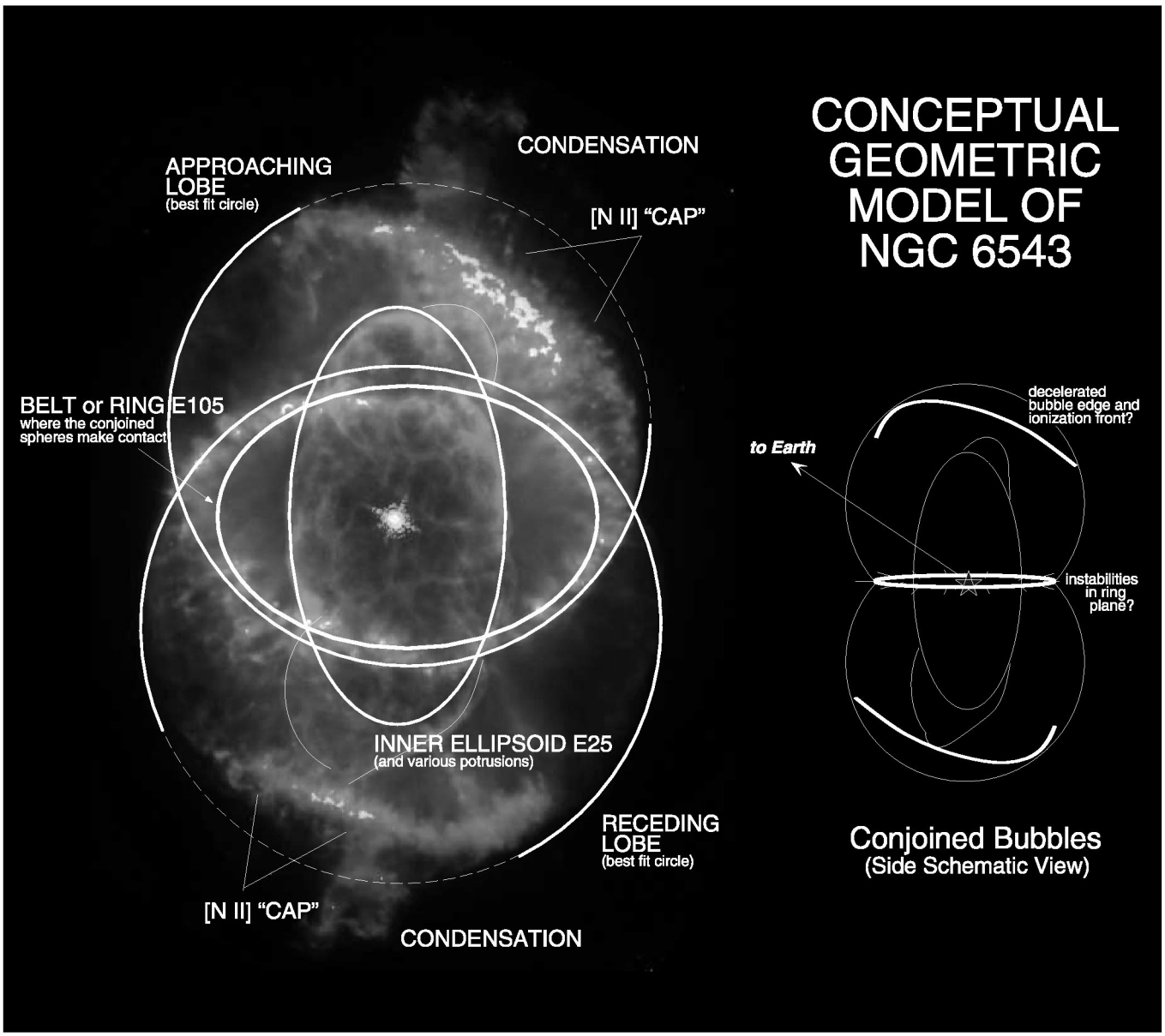

FIG. 6.—Geometric model of NGC 6543. *Left*, its possible appearance if tilted about 30° shown in projection on a combined [N II] and [O III] image; *right*, a plan view of the model.

angular expansion rate of E25 is predicted to be largest along its major axis. Rather, just the reverse is seen. The kinematic age of the tips of E25 is roughly twice as large as the kinematic age of its waist. If the observed trends continue, the E25 ellipsoid will evolve to become increasingly less prolate.

To rescue the concept of E25 as a thermally expanding bubble, one might argue that, although the tips of the bubble originally expanded much faster than its waist, the tips have now displaced and accreted considerable amounts of gas with lower specific momentum and have been decelerated. Alternately, the gas behind the tips may have cooled adiabatically, so the thermal pressure driving the expansion has abated.

Conjoined bubbles.—Almost certainly the conjoined bubbles represent the projected edges of a pair of bubble-like shells conjoined along their waist. Along its waist, a ruffled and slightly irregular series of ragged, low-ionization, elongated knots (E105) seems to point away from the nucleus. These knots may be the result of an instability formed as the edges of the expanding bubbles pinch and compress the trapped gas in their waist, like the blades of a pair of scissors. Alternately, they are ablation flows from dense neutral knots subjected to ionizing radiation (Mellema et al. 1998; Redman & Dyson 1999).

Although E25 has counterparts in many other planetary nebulae, the conjoined bubbles do not. The closest analogs may be NGC 7027 and some bipolar nebulae, such as NGC 650-1, 2371-2, and 6309. Interestingly, the conjoined bubbles also mimic η Carinae, except that the waist of the latter object looks like a large thin disk with radial streaks, and its figure eight is more pinched. If η Carinae follows the pattern of decreasing expansion with radius that presently characterizes the conjoined bubbles, then it is not difficult to imagine that its overall morphology will evolve over time to resemble the conjoined bubbles. Dwarkadas & Balick

(1998) showed how this might happen if the hydrodynamic evolution of the system is dominated by thermal expansion and adiabatic cooling.

Historical Evolution.—One key fact is that the waists of the conjoined bubbles E105 and E25 have the same kinematic age within our error bars. Hence, E25 and the conjoined bubbles formed at roughly the same time. Based on the increasing kinematic age with radial distance from the nucleus, it appears that E25 is overtaking some of the more distant nebular regions such as the tips of E25 and the caps DD′.

We propose a fairly simple framework for understanding the evolution of the core of NGC 6543. About 1000 yr ago, the star ejected a pulse of material that now forms the conjoined bubbles. However, the absence of limb brightening along the edges of the conjoined bubbles (except at DD′) suggests that the ejection event filled the interior with low-density gas. For example, this might have happened if the gas formed a shock that left some of the outflowing gas in a hot state.

Starting shortly after the pulse of mass ejection, the nucleus has been blowing a high-speed wind, perhaps much like the wind observed today: $\dot{M}_{\rm wind} \sim 10^{-7.4} M_{\odot}$ yr^{-1} and $v_{\rm wind} \sim 1900$ km s^{-1} (Perinotto, Cerruti-Sola, & Lamers 1989). This wind has swept into the interior of the expanding conjoined bubbles. It has displaced and plowed the upstream gas and has formed feature E25; therefore, E25 defines the "realm" of the wind-affected portion of the core of the nebula.

E25 is now seen as a prolate balloon pushing into the interior of the conjoined bubbles, fastest near the equator and decelerating toward the poles. As we noted before, the plowing of slower upstream gas and adiabatic cooling inside the tips may have slowed the expansion of E25 along its major axis.

The upstream portions of the conjoined bubbles have yet to know of the existence of E25. Thus the morphology of the conjoined bubbles is a result of events that shaped it initially. This feature "remembers" its origins. Its pinched waist suggests that a thin, dense disk shaped it into a bipolar when it was formed. E105 is the remnant of this disk.

This fanciful scenario fails to account for the symmetrically placed caps, condensations, and jets of NGC 6543. We can only conjecture that the caps are dense, neutral material left behind by an even earlier ejection of mass. Their low specific momentum and neutral, dense gas impede the polar growth of the conjoined bubbles and, at the same time, cause dense ionization fronts to form. The origins of the condensations and jets are even less obvious. We shall return to these issues in a later paper, which discusses the detailed ionization structure of the nebula.

5. SUMMARY

The excellent agreement of each of the three methods presented confirms that we have, for the first time, measured the optical expansion parallax of a PN and that our error estimates are adequate. We have shown that accurate measurements of the expansion of nebular features are readily obtainable with the WFPC2 camera with a reasonable time baseline. We have further shown that the E25 major axis, the polar caps, the polar condensations, and the conjoined bubbles are all expanding significantly slower than expected of a Hubble-like expansion. This result is confirmed in both the [O III] and [S II] images and indicates a region where ejected gas is either decelerating, left behind from an earlier epoch, or both.

Combining the proper motion of bright fiducials of the nebula with corresponding spectroscopically obtained radial expansion velocities (MS92) has allowed us to determine the distance to NGC 6543 of 1001 ± 269 pc. Our deduced kinematic age of the brightest inner parts of the core of the nebula, based on three measurements along the minor axis of the tilted prolate ellipsoid E25, is 1039 ± 259 yr. The outer regions, which resemble a pair of conjoined bubbles with a large waist, have longer kinematic ages.

A heuristic and highly conceptual explanation of the evolution of these features is as follows: A major outburst occurred a thousand years before today's nebula formed. Even earlier outbursts produced the huge halo that surrounds NGC 6543, the polar caps, and other features beyond a radius of $\sim 20''$ from the nucleus. These debris form the environment for the latest ejection.

The major outburst formed a dense equatorial disk, of which the remnants are E105. In addition, the ejected gas was shaped by this disk into a pair of expanding bubbles, which join at E105. The conjoined bubbles were created in such a way that their interiors are uniform and probably in a hot state. These bubbles are expanding and adiabatically cooling.

Stellar winds began to blow at high speeds shortly after the latest massive outburst. These have created an overpressured hot bubble, which expands into the interior of the conjoined bubbles. The bubble attained a prolate geometry by rapid expansion along its polar direction. The subsequent evolution of the bubble has formed E25.

Like many other interior bubbles in PNe, E25 is forming lumps on its surface, perhaps the result of the buckling of its thin expanding shell. The expansion of the tips of the prolate bubble has displaced and accreted material of lower specific momentum, so the tips have decelerated much more than the waist. E25 is therefore becoming less prolate as it expands.

In the future E25 may overtake the conjoined bubbles. When this occurs, Rayleigh-Taylor instabilities will set in, shredding the remnants of the nebula and forming a clumpy halo perhaps much like the larger one that presently surrounds NGC 6543 (see, e.g., Balick et al. 1992).

The ongoing GO 7501 program has selected 30 PNe for WFPC2 observations for its ongoing multiepoch expansion parallax program. First-epoch observations are nearly complete. Subsequent observations will allow accurate expansion parallax distance measurements of these PNe. Third-epoch observations of NGC 6543 are planned for late in the year 2000, when the observing configuration of the observations by Harrington & Borkowski (1994; GO 5403) will be replicated in the bright, complementary nebular lines of [O III] and [N II] as closely as possible. This observation should provide excellent data spanning 6 years under highly controlled conditions, allowing even more accurate measurements of the expansion patterns and the distance to NGC 6543.

We are extremely grateful to Virginia Player for her diligent efforts in making astrometric measurements for our analyses. We are most grateful to the Space Telescope Science Institute for providing archived data used in this study. Support for this work was provided by NASA through grant GO 7501 from the Space Telescope Science Institute.

REFERENCES

Balick, B., Gonzalez, G., Frank, A., & Jacoby, G. J. 1992, ApJ, 392, 582
Balick, B., Wilson, J., & Harrington, J. P. 1999, in preparation
Balick, B., Alexander, J., Hajian, A. R., Terzian, Y., Perinotto, M., & Patriarchi, P. 1998, AJ, 116, 360
Cahn, J. H., Kaler, J. B., & Stanghellini, L. 1992, A&AS, 94, 399
Castor, J. I., Lutz, J. H., & Seaton, M. J. 1981, MNRAS, 244, 521
Ciardullo, R., Jacoby, G. H., & Ford, H. C. 1988, PASP, 100, 1218
Cudworth, K. M. 1974, AJ, 79, 1384
Daub, C. T. 1982, ApJ, 260, 612
Dwarkadas, V., & Balick, B. 1998, AJ, 116, 829
Gómez, Y., Rodríguez, L. F., & Moran, J. M. 1993, ApJ, 416, 620
Hajian, A. R., & Terzian, Y. 1996, PASP, 108, 258
Hajian, A. R., Terzian, Y., & Bignell, C. 1993, AJ, 106, 1965
———. 1995, AJ, 109, 2600
Harrington, J. P., & Borkowski, K. J. 1994, BAAS, 26, 1469
Haryadi, C., & Seaquist, E. R. 1998, AJ, 115, 2466
Heap, S. R., & Augensen, H. J. 1987, ApJ, 313, 268
Icke, V., Balick, B., & Frank, A. 1992, A&A, 253, 224
Masson, C. R. 1986, Astrophys. Lett., 302, L27
———. 1989a, ApJ, 336, 294
———. 1989b, ApJ, 346, 243
Mellema, G., Raga, A. C., Cantó, J., Lundqvist, P., Balick, B., Steffen, W., & Noriega-Crespo, A. 1998, A&A, 331, 335
Miranda, L. F., & Solf, J. 1992, A&A, 260, 397 (MS92)
Morse, J. A., Davidson, K., Bally, J., Ebbets, D., Balick, B., & Frank, A. 1998, AJ, 116, 2443
Perinotto, M., Cerruti-Sola, M., & Lamers, H. J. G. L. M. 1989, ApJ, 337, 382
Redman, M. P., & Dyson, J. E. 1999, MNRAS, 302, 17
Shklovsky, I. S. 1956, AZh, 33, 22
Terzian, Y. 1997, in IAU Symp. 180, Planetary Nebulae, ed. H. J. Habing & H. J. G. L. M. Lamers (Dordrecht: Kluwer)